Bifurcation analysis of a Morris–Lecar neuron model

Article *in* Biological Cybernetics · January 2014

DOI: 10.1007/s00422-013-0580-4 · Source: PubMed

3 authors, including:

Xuanliang Liu
South China University of Technology
28 PUBLICATIONS **138** CITATIONS
SEE PROFILE

Liu Shenquan
South China University of Technology
81 PUBLICATIONS **168** CITATIONS
SEE PROFILE

Biol Cybern (2014) 108:75–84
DOI 10.1007/s00422-013-0580-4

ORIGINAL PAPER

Biological Cybernetics

Bifurcation analysis of a Morris–Lecar neuron model

Congmin Liu · Xuanliang Liu · Shenquan Liu

Received: 2 October 2013 / Accepted: 10 December 2013 / Published online: 17 January 2014

Abstract In this paper, we investigate the dynamical behaviors of a Morris–Lecar neuron model. By using bifurcation methods and numerical simulations, we examine the global structure of bifurcations of the model. Results are summarized in various two-parameter bifurcation diagrams with the stimulating current as the abscissa and the other parameter as the ordinate. We also give the one-parameter bifurcation diagrams and pay much attention to the emergence of periodic solutions and bistability. Different membrane excitability is obtained by bifurcation analysis and frequency-current curves. The alteration of the membrane properties of the Morris–Lecar neurons is discussed.

Keywords Morris–Lecar model · Limit cycle · Bifurcation · Bistability

1 Introduction

Action potentials are generated by neurons with the purpose of transmitting information through the nervous system (Koch 1999; Izhikevich 2007). According to the firing patterns of action potentials and frequency-current curves, Hodgkin proposed three basic classes of neuronal excitability (Hodgkin 1948). The distinction among classes 1, 2, and 3 excitability has been proved extremely useful. Class 1 excitable neurons can smoothly encode the strength of an input into the output firing frequency; Class 2 neurons cannot do that, and they fire in a relatively narrow frequency band; Class 3 neurons cannot exhibit sustained spiking activity, so Hodgkin regarded them as "sick" or "unhealthy," but "healthy" Class 3 neurons have been described in the auditory brainstem neurons [e.g., in the medial superior olive (Smith 1995)], dorsal horn of the spinal cord (Prescott and Koninck 2002), dorsal root ganglia (Sculptoreanu and Groat 2007), etc. Many papers have studied Hodgkin's classes 1 and 2 excitability by the mechanisms of bifurcations and phase space analysis (FitzHugh 1955; Rinzel and Ermentrout 1989; Gutkin and Ermentrout 1998; Izhikevich 2000, 2007; Tsumoto et al. 2006; Tsuji et al. 2007; Prescott et al. 2008). Class 1 excitability is concerned with a saddle-node on invariant circle bifurcation in which the oscillation emerges with zero frequency. On the other hand, Class 2 excitability is observed when a rest potential loses stability via an Andronov-Hopf bifurcation, which is characterized by the oscillation emerging with nonzero frequency. Class 3 excitability occurs when the resting state remains stable, and no bifurcation appears. For the Morris–Lecar model (Morris and Lecar 1981), Rinzel and Ermentrout (1989) studied classes 1 and 2 excitability by changing stimulating current. They found that the bifurcations in the generation of the repetitive firing change from the saddle-node bifurcation to the subcritical Hopf bifurcation. Tsumoto et al. (2006) gave a global view of the bifurcation mechanism of the Morris–Lecar model. They investigated one- or two-parameter bifurcation diagrams of the model.

In this paper, we study the dynamics of a Morris–Lecar model from Prescott et al. (2008). The model parameters of this paper are different from the previously used parameters in Morris–Lecar models. We give the one- and two-parameter bifurcation analyses of this model. We investigate the excitability from the viewpoint of bifurcation. We also discuss the alteration of the membrane properties and the bistability of the Morris–Lecar model.

The paper is organized as follows: In Sect. 2, we describe the Morris–Lecar model and list the tools for computer sim-

C. Liu · X. Liu (✉) · S. Liu
Department of Mathematics, South China University of Technology, Guangzhou 510640, China
e-mail: liuliang@scut.edu.cn

ulations. The results of the bifurcation diagrams and phase portraits are shown in Sect. 3. Finally, the conclusions and the discussions are given in Sect. 4.

2 Model and tools

Prescott et al. (2008) consider a Morris–Lecar model, which is described by

$$\begin{aligned} C\frac{\mathrm{d}V}{\mathrm{d}t} &= I_{\mathrm{stim}} - g_{\mathrm{fast}} m_\infty(V)(V - E_{\mathrm{Na}}) - g_{\mathrm{slow}} w(V - E_{\mathrm{k}}) \\ &\quad - g_{\mathrm{leak}}(V - E_{\mathrm{leak}}), \\ \frac{\mathrm{d}w}{\mathrm{d}t} &= \phi_w \frac{w_\infty(V) - w}{\tau_w(V)}, \end{aligned} \tag{1}$$

where V represents the fast activation variable; w is the slower recovery variable; I_{stim} is the stimulating current that is assumed to be temporally constant. The system parameters E_{Na}, E_{k}, and E_{leak} represent equilibrium potentials of Na^+, K^+, and leak currents; g_{fast}, g_{slow}, and g_{leak} denote the maximum conductances of corresponding fast, slower, and leak current, respectively. The steady-state activation functions and the time constant are given by the following:

$$m_\infty(V) = 0.5\left[1 + \tanh\left(\frac{V - \beta_m}{\gamma_m}\right)\right],$$

$$w_\infty(V) = 0.5\left[1 + \tanh\left(\frac{V - \beta_w}{\gamma_w}\right)\right],$$

$$\tau_w(V) = \frac{1}{\cosh\left(\frac{V-\beta_w}{2\gamma_w}\right)}.$$

The following parameter values are the same as in Prescott et al. (2008):

$$\begin{aligned} &E_{\mathrm{Na}} = 50\,\mathrm{mV},\ E_{\mathrm{k}} = -100\,\mathrm{mV},\ E_{\mathrm{leak}} = -70\,\mathrm{mV}, \\ &g_{\mathrm{fast}} = 20\,\mathrm{mS/cm^2},\ g_{\mathrm{slow}} = 20\,\mathrm{mS/cm^2},\ g_{\mathrm{leak}} = 2\,\mathrm{mS/cm^2}, \\ &\phi_w = 0.15,\ C = 2\,\mu\mathrm{F/cm^2},\ \gamma_m = 18\,\mathrm{mV}, \end{aligned}$$

the other parameters I_{stim}, β_m, β_w, γ_w are varied in the next section.

When varying the parameter β_m or β_w, the Morris–Lecar model can exhibit classes 1, 2, and 3 excitability based on their frequency-current curves. In this paper, we treat I_{stim} as a main control parameter and analyze two-parameter bifurcations in the parameter plane of I_{stim} as the abscissa and one of the parameters β_m and β_w as the ordinate. We also give the one-parameter bifurcation diagrams, frequency-current curves, phase portraits, and waveforms of the Morris–Lecar model.

The model has been integrated by the fourth-order Runge–Kutta method with a time step of 0.01. The integration, bifurcation analysis, and phase plane analysis were performed using the parameter continuation software MATCONT (Kuznetsov et al. 2010) and MATLAB.

3 Results

In this section, we give the numerical results from the bifurcation analysis of Morris–Lecar model (1). We use the following symbols in the bifurcation diagrams of this paper: SN_i and H_i, $(i = 1, 2)$ represent for the saddle-node bifurcation and Hopf bifurcation of an equilibrium point, respectively; LPC_i, $(i = 1, 2)$ for the tangent bifurcation of limit cycles; Hom_i, $(i = 1, 2)$ for the homoclinic bifurcation; GH, BT, and CP for the generalized Hopf bifurcation, the Bogdanov–Takens bifurcation, and the cusp bifurcation of an equilibrium point, respectively. The meanings of these bifurcations can be referred to Kuznetsov (1998) or Guckenheimer and Holmes (1983). In one-parameter bifurcation diagrams, the symbols $\mathrm{V}_{\max}$ and $\mathrm{V}_{\min}$ denote the maximum value and the minimum value of V of the limit cycles, respectively. The solid blue curves represent the values of V at the stable equilibria (or stable limit cycles), and the dashed blue curves denote the values of V at the unstable equilibria (or unstable limit cycles).

In the following, we will discuss bifurcation phenomena observed in two-parameter bifurcation diagrams of $(I_{\mathrm{stim}}, \beta_m)$ and $(I_{\mathrm{stim}}, \beta_w)$-planes, respectively.

3.1 Bifurcations in the $(I_{\mathrm{stim}}, \beta_m)$-plane

Let $\beta_w = -10\,\mathrm{mV}$, $\gamma_w = 13\,\mathrm{mV}$. All other parameters are as indicated in Sect. 2. Figure 1a is the two-parameter bifurcation diagram in the $(I_{\mathrm{stim}}, \beta_m)$-plane. Figure 1b–d are enlarged bifurcation diagrams around LPC_1, BT, and LPC_2, respectively. In Fig. 1, the yellow region indicates parameters at which a stable limit cycle exists; in green region, three equilibrium points coexist. In the following, we account for each bifurcation mechanism along lines l_1, l_2, l_3, and l_4 in Fig. 1a.

Figure 2a shows a one-parameter bifurcation diagram along the line l_1 with $\beta_m = 0$ in Fig. 1 (or an enlarged bifurcation diagram Fig. 1). If I_{stim} is relatively small, then the Morris–Lecar model (1) has a stable equilibrium point EP. An example of which is shown in Fig. 3a. By increasing I_{stim}, a pair of limit cycles is generated by the tangent bifurcation LPC_1. One of them is a stable limit cycle, which corresponds to repetitive firing in the Morris–Lecar model (1). It coexists with the stable equilibrium point; namely, there is a bistability in the narrow range between the bifurcation point LPC_1 and the subcritical Hopf bifurcation point H_1. An example of the bistability is shown in Fig. 3b. After the Hopf bifurcation H_1, the stable limit cycle remains a unique attractor. An example of which is shown in Fig. 3c.

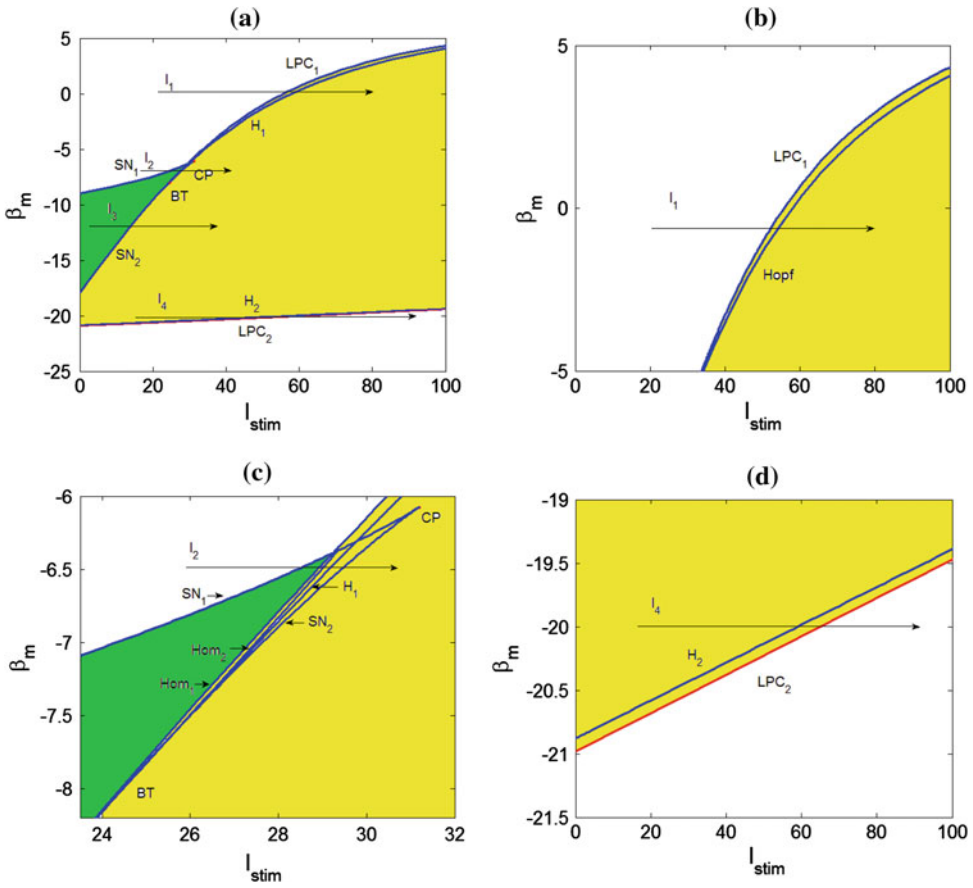

Fig. 1 **a** Two-parameter bifurcation diagram in the $(I_{\text{stim}}, \beta_m)$-plane. All parameters are as indicated in Sect. 2 with $\beta_w = -10\,\text{mV}$ and $\gamma_w = 13\,\text{mV}$. The *yellow region* indicates parameters at which a stable limit cycle exists. In *green region*, three equilibrium points coexist. The values of β_m in l_1, l_2, l_3, l_4 are $0, -6.5, -12, -20$, respectively. **b**–**d** are the enlarged bifurcation diagrams around l_1, l_2, l_4 of **a**, respectively. Detailed analysis of **b**–**d** is given later (color figure online)

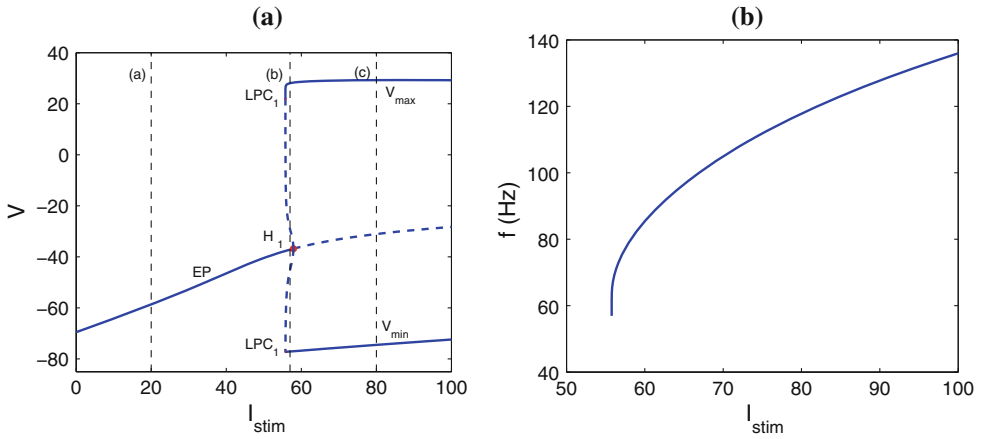

Fig. 2 **a** One-parameter bifurcation diagram along the line l_1 ($\beta_m = 0$). The *solid and dashed blue curves* represent the values of V at the equilibria (or the maximum and minimum values of V of limit cycles), stable and unstable, correspondingly. The *vertical dashed lines* represent $I_{\text{stim}} = 20, 57, 80$, respectively. By increasing I_{stim}, the model will undergo the tangent bifurcation of limit cycles (LPC_1) and Hopf bifurcation (H_1). **b** Frequency f as a function of I_{stim}. This function is discontinuous, and action potentials are generated in a certain frequency band, which is the typical property of Class 2 excitability

Figure 2b shows the frequency-current ($f - I_{\text{stim}}$) curve alone the line l_1 in Fig. 1a. We see that the repetitive firing with a nonzero frequency appears via the subcritical Hopf bifurcation, which is the typical property of Class 2 excitability.

Figure 4b shows a one-parameter bifurcation diagram along the line l_2 with $\beta_m = -6.5$ in Fig. 4a. If I_{stim} is relatively small, then the system (1) has a stable equilibrium point EP. By increasing I_{stim}, an unstable node point EP_1 and a saddle point EP_2 are generated from the saddle-node bifur-

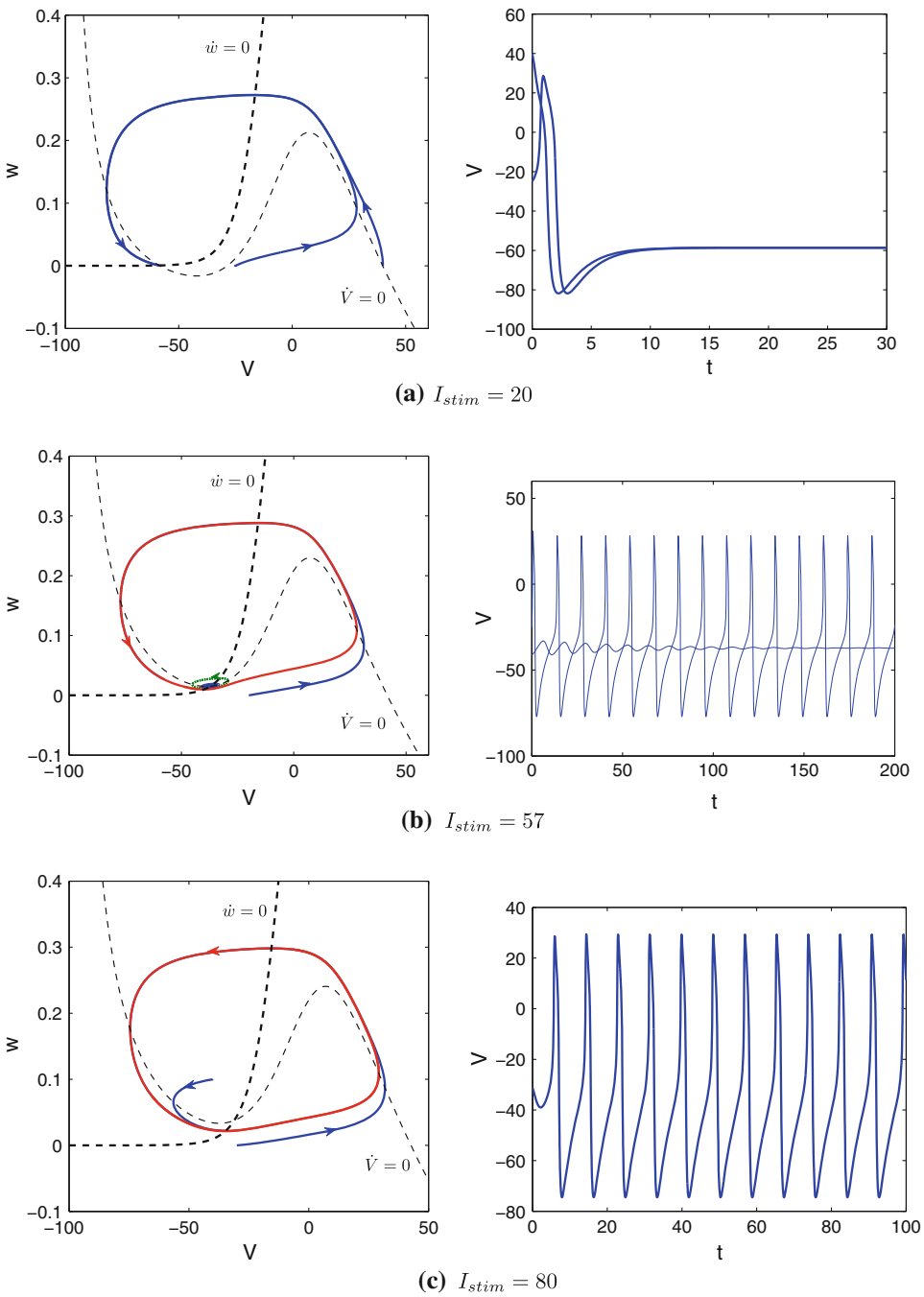

Fig. 3 Examples of phase portraits (*left*) and waveforms (*right*) when $\beta_m = 0$.*Red and dark green closed curves* in phase portraits (**b**), and (**c**) denote stable and unstable limit cycles, respectively. *Arrows* indicate directions of trajectories. *Light and heavy dashed curves* indicate V- and w-nullclines of model (1) (color figure online)

cation of the equilibrium point SN_1. By further increasing I_{stim}, there is a homoclinic bifurcation point Hom_1 [labeled by (c) in Fig. 4b], which corresponds to a large homoclinic orbit. After the bifurcation point Hom_1, the homoclinic orbit is destroyed and a stable limit cycle appears. The next bifurcation is another kind of homoclinic bifurcation Hom_2 [labeled by (d) in Fig. 4b], which corresponds to a small homoclinic orbit. After the homoclinic bifurcation Hom_2, an unstable limit cycle appears and it shrinks to a subcritical Hopf bifurcation point H_1; after that, an unstable equilibrium point EP_3 and a saddle point EP_2 get close to each other, coalesce at the saddle-node bifurcation point SN_2, and then disappear. By further increasing I_{stim}, the Morris–Lecar model (1) has a unique unstable equilibrium EP_1 and a stable limit cycle. It is easy to see that the Morris–Lecar neuron is bistable between the homoclinic bifurcation Hom_1 and the Hopf bifurcation H_1. After the Hopf bifurcation H_1, the stable limit cycle remains a unique attractor.

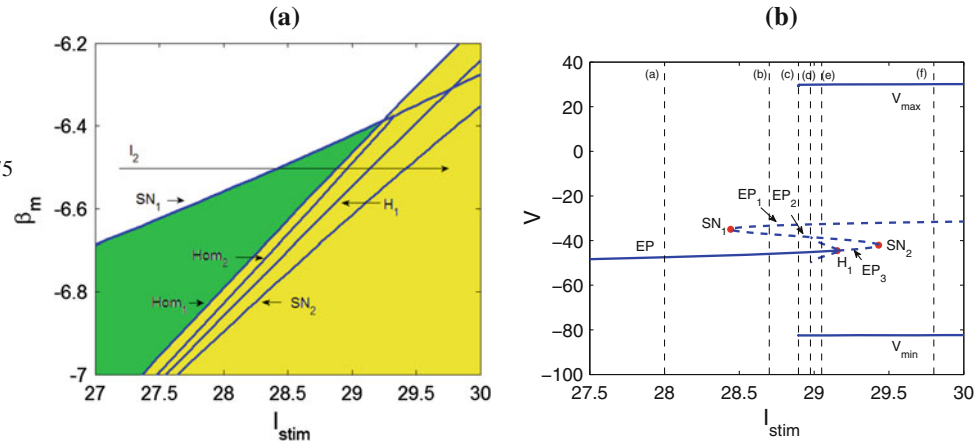

Fig. 4 **a** An enlarged bifurcation diagram around the line l_2 in Fig. 1c ($\beta_m = -6.5$). **b** One-parameter bifurcation diagram along the line l_2. The *vertical dashed lines* represent $I_{\text{stim}} = 28, 28.7, 28.895111, 28.97575$ respectively. In **a** and **b**, by increasing I_{stim}, the model has saddle-node bifurcation of equilibria (SN_1, SN_2), Hopf bifurcation (H_1), a large homoclinic orbit bifurcation (Hom_1), and a small homoclinic orbit bifurcation (Hom_2)

Hence, the Morris–Lecar neuron is monostable. Examples are shown in Fig. 5a–f. The values of I_{stim} labeled by (a)–(f) in Fig. 4b correspond to the phase portraits shown in Fig. 5a–f.

Figure 6a shows a one-parameter bifurcation diagram along the line l_3 with $\beta_m = -12$ in Fig. 1a. As I_{stim} increasing, the stable equilibrium EP_1 and the saddle equilibrium EP_2 get closer to each other, and they coalesce at the saddle-node bifurcation point SN_2 and then disappear. After the saddle-node bifurcation SN_2, a stable limit cycle is generated from a saddle-node on invariant circle bifurcation. Figure 7a–c illustrate phase portraits and waveforms before and after the saddle-node on invariant circle bifurcation. The values of I_{stim} labeled by a–c in Fig. 6a correspond to the phase portraits in Fig. 7a–c, respectively.

Figure 6b shows the frequency-current ($f - I_{\text{stim}}$) curve alone the line l_3 in Fig. 1a. We see that the repetitive firing starts with the zero frequency occurring via a saddle-node on invariant circle bifurcation. Hence, the Morris–Lecar neuron exhibits the property of the Class 1 excitability.

The bifurcation mechanism along line l_4 in Fig. 1a (or an enlarged bifurcation diagram Fig. 1d) is similar to those along line l_1 in Fig. 1a. Model (1) goes through the same bifurcations along l_1 and l_4, but in the opposite direction. The one-parameter bifurcation diagram and the frequency-current ($f - I_{\text{stim}}$) curve are shown in Fig. 8a, b, respectively. From the frequency-current curve in Fig. 8b, we see that the frequency at the transition "spiking→ resting" stops at a nonzero value. According to Izhikevich (2000) or Izhikevich (2007), this is a Class 2 spiking.

Along the line with $\beta_m = -23$ in Fig. 1a (not shown in Fig. 1a), the resting state remains stable for I_{stim} varying from 0 to 100 mV; no bifurcation occur, which corresponds to Class 3 excitability.

3.2 Bifurcations in the ($I_{\text{stim}} - \beta_w$)-plane

Let $\beta_m = -1.2$ mV, $\gamma_w = 10$ mV. All other parameter values are the same as in Sect. 2. Figure 9a is the two-parameter bifurcation diagram of Morris–Lecar model (1) in (I_{stim}, β_w) -plane. Figure 9b is an enlarged diagram in the dashed box of Fig. 9a. The bifurcation diagram Fig. 9a is almost the same as the bifurcation diagram Fig. 1a of Tsumoto et al. (2006), except for (β_m, γ_w) in the dashed box of Fig. 9a. Therefore, we only consider the bifurcation mechanism in Fig. 9b.

Figure 10a shows a one-parameter bifurcation diagram along the line l_1 with $\beta_w = -18.5$ in Fig. 9b. When I_{stim} is relatively small, the model has exactly a stable equilibrium point EP. An example of which is shown in Fig. 11a. By increasing I_{stim}, a pair of limit cycles is generated from the tangent bifurcation LPC_1. Moreover, there is a bistability in the narrow range between the tangent bifurcation point LPC_1 and the supercritical Hopf bifurcation point H_2 in Fig. 10a; namely, a stable limit cycle coexists with a stable equilibrium point. An example of bistability is shown in Fig. 11b. By further increasing I_{stim}, the equilibrium point loses stability. Model (1) has three limit cycles between the Hopf bifurcation point H_2 and the tangent bifurcation point LPC_2, two of which are stable, and the another one is unstable. Hence, there is also a bistability in the narrow range. An example of which is shown in Fig. 11c. After the tangent bifurcation LPC_2, the stable limit cycle remains a unique attractor. An example of which is shown in Fig. 11d.

Figure 10b shows a one-parameter bifurcation diagram along the line l_2 with $\beta_w = -20.5$ in Fig. 9b. The Hopf bifurcation H_2 is between LPC_1 and LPC_2 in Fig. 10a, but it is in front of LPC_1 in Fig. 10b. The bifurcation mechanisms of model (1) along the lines l_1 and l_2 in Fig. 9b are similar to each other. Model (1) is bistable in the narrow range between the tangent bifurcation LPC_1 and LPC_2 in Fig. 10b.

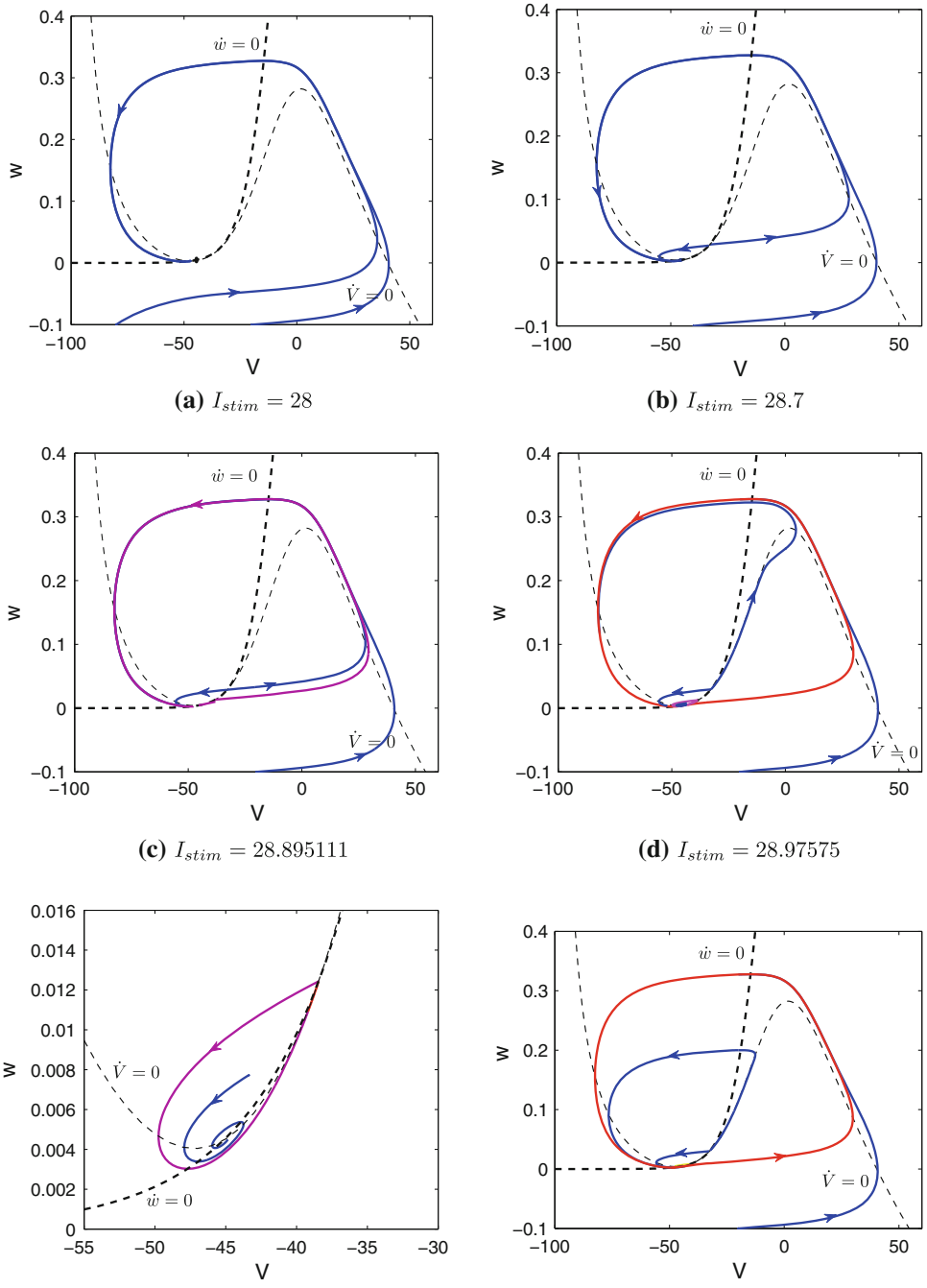

Fig. 5 Examples of phase portraits observed in Eq. (1) with $\beta_m = -6.5$. *Red and dark green closed curves* in phase portraits denote stable and unstable limit cycles, respectively. *Purple curves*in phase portraits (**c**), (**d**), and (**d1**) indicate large and small homoclinic orbits, respectively (color figure online)

4 Conclusions and discussions

The aim of this paper is to investigate dynamics of a Morris–Lecar model. By changing I_{stim}, β_m, and β_w, we give two-parameter and one-parameter bifurcation analyses of the Morris–Lecar model. We have found that the Morris–Lecar model can exhibit the properties of classes 1, 2, and 3 excitability and bistability.

For the study of Morris–Lecar model, FitzHugh (1955) discussed stable solutions by changing the system parameters I_{ext}, ϕ, $\bar{g}_{\text{ca}}$, V_3, V_4 (which correspond to I_{stim}, ϕ_w, g_{fast}, β_w, γ_w in Morris–Lecar model (1), respectively). They presented that the membrane properties of classes 1 and 2 correspond to repetitive firing oscillations generated by a saddle-node and a subcritical Hopf bifurcation of equilibrium points, respectively. Tsumoto et al. (2006) investigated

Fig. 5 continued

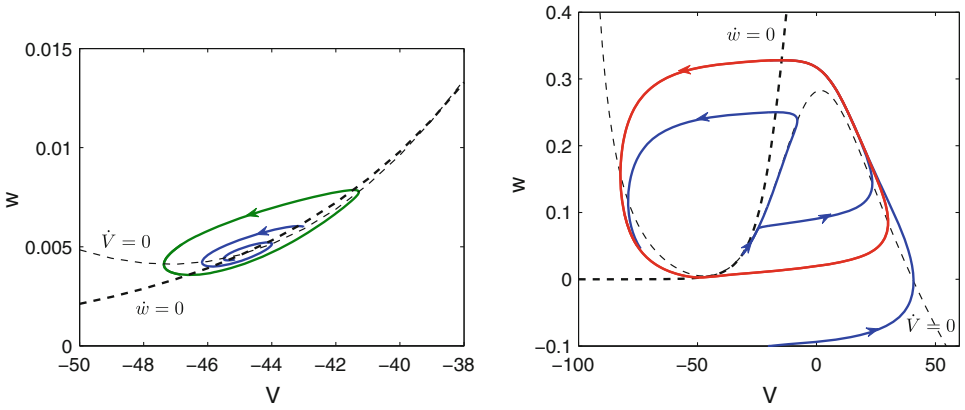

(e1) Enlargement figure of (e) near stable equilibrium

(f) $I_{stim} = 29.8$

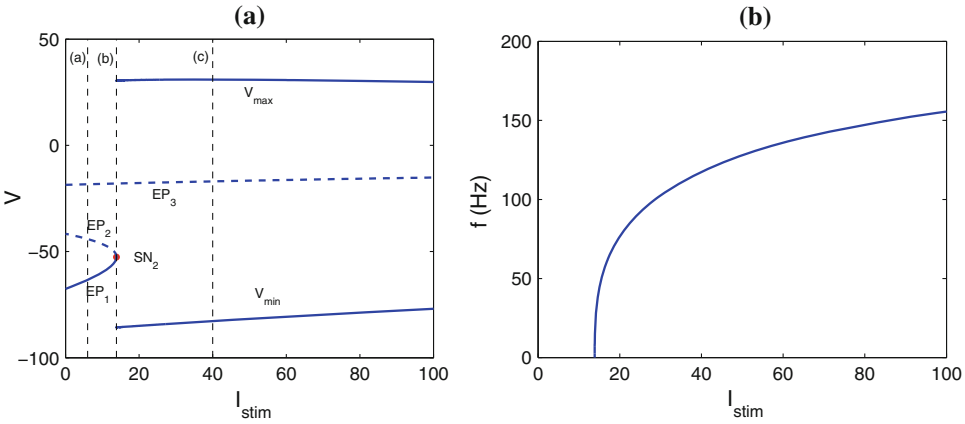

Fig. 6 **a** One-parameter bifurcation diagram along the line l_3 ($\beta_m = -12$). A saddle-node on invariant circle (SNIC) bifurcation occurs, i.e., the model has a bifurcation of homoclinic orbits to saddle-node point (SN_2). The *vertical dashed lines* represent $I_{\text{stim}} = 6, 13.849841, 40$, respectively. **b** Frequency f as a function of I_{stim}. This function is continuous. Action potentials are generated with arbitrarily low frequency; this is the typical property of Class I excitability

detailed bifurcations of invariant sets in the parameter space $I_{\text{ext}}, \phi, \bar{g}_{\text{ca}}, V_3, V_4$. They gave the two-parameter and one-parameter bifurcation analysis of the Morris–Lecar model, and presented the mechanism of global transition between Class 1 and Class 2 from the bifurcation point of view. Prescott et al. (2008) gave the one-parameter bifurcation analysis of a Morris–Lecar model in spinal lamina I neurons. They analyzed classes 1, 2, and 3 excitability by changing the stimulating current. In this paper, we have studied the two-parameter bifurcation in (I_{stim}, β_m) parameter plane; the bifurcation diagram is shown in Fig. 1a. When β_m decrease, classes 1, 2, and 3 excitability will vary. We have shown that the Morris–Lecar model can exhibit classes 2, 1, and 3 excitability when the parameters (I_{stim}, β_m) of model (1) vary along l_1, l_3, and the line with $\beta_m = -23$ in Fig. 1a, respectively. Between the lines l_1 and l_3, the model undergoes the Bogdanov–Takens bifurcation, which is important to switch between Class 2 and Class 1 excitability. Izhikevich (2000) suggested the classification of repetitive spiking based on the frequency as oscillations terminate. Namely, Class 1 spiking systems exhibit terminating oscillations having arbitrary low frequency; Class 2 spiking systems exhibit oscillations that terminate with a nonzero frequency. According to this classification of repetitive spiking, we conclude that the class of excitability coincides with the class of spiking when model (1) along with l_1, l_3, and l_4 in Fig. 1a, but the neuron exhibits Class 2 excitability and Class 1 spiking along l_2 in Fig. 1a.

It is easy to see that β_m is a parameter determining the property of the membrane excitability of the Morris–Lecar model, which has the same function as β_w (or V_3) in Prescott et al. (2008) (or Tsumoto et al. 2006). β_m and β_w were half-maximal activation of the fast current (I_{fast}) and slow current (I_{slow}), respectively. I_{fast} and I_{slow} represent the sum of all ion currents with fast- and slow-gating kinetics, respectively. Grouping currents with similar kinetics is a method for reducing dimensionality (Kepler et al. 1992). The low-dimensional model is better for mathematical analysis, but the higher-dimensional model is better for biological interpretation. For example, we can ungroup I_{slow} into parts which include the delayed rectifier K^+ current $I_{k,dr}$ and a subthreshold current I_{sub}. This converts the model from 2D to 3D and makes it more biophysically realistic.

We also consider the bistability in this paper. Bistable systems have an important neurocomputational property: They

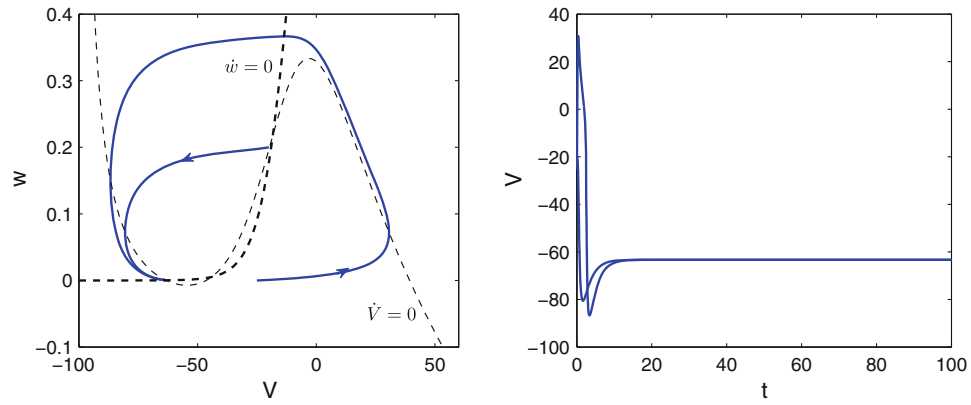

(a) $I_{stim} = 6$

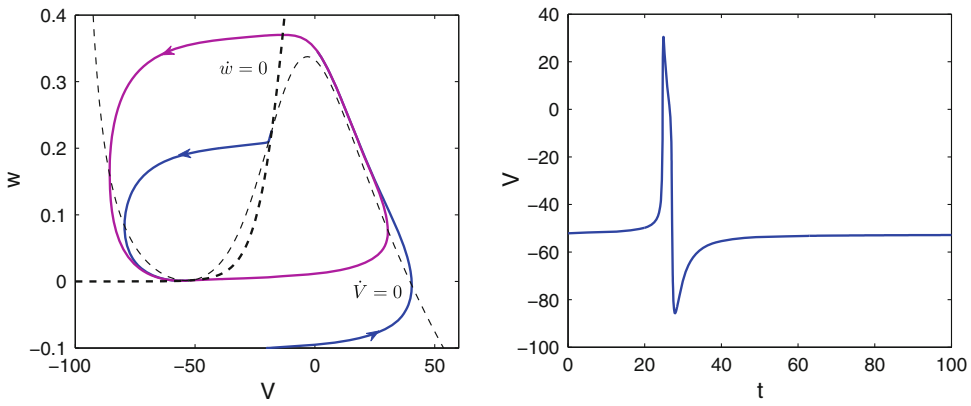

(b) $I_{stim} = 13.849841$

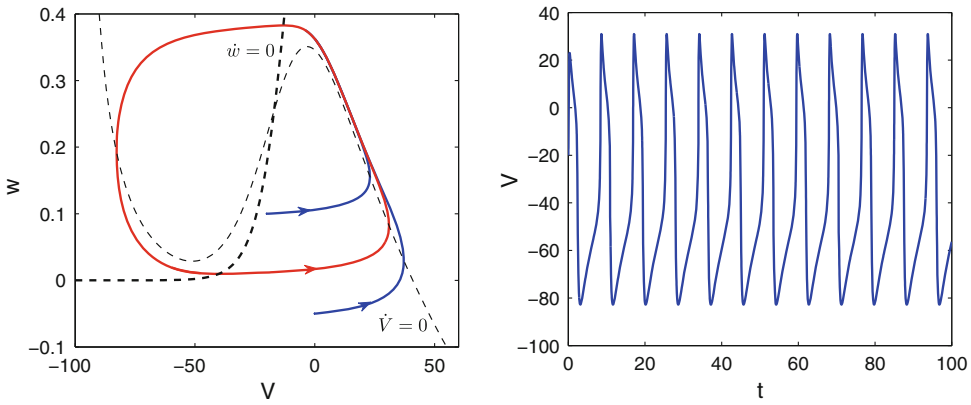

(c) $I_{stim} = 40$

Fig. 7 Examples of phase portraits (*left*) and waveforms (*right*) when $\beta_m = -12$. The *purple curve and red closed curve* in phase portraits (**b**) and (**c**) denote homoclinic orbit and stable limit cycle, respectively (color figure online)

can be switched from one state to the other by an appropriate stimulation. We have found that the Morris–Lecar model (1) has bistability along the line l_1, l_2, and l_4 in Fig. 1a and along l_1 and l_2 in Fig. 9b for some parameters, respectively. Along the l_1 and l_2 in Fig. 9b, the neuron has two different kinds of bistability. One kind is coexistence of a stable equilibrium point and a stable limit cycle; another kind is coexistence of two stable limit cycles. Therefore, changing the initial state of neurons with other stimuli, such as noise, or adding an adaptation current, for example, calcium-activated K^+ current or voltage-activated M-type K^+ current, will lead the neurons changing from rest to tonic-spiking, or from the small amplitude tonic-spiking to large amplitude tonic-spiking.

For the analysis in $(I_{\text{stim}}, \beta_w)$ parameter plane, we only discuss the different parts between the bifurcation diagram in Fig. 9a and the bifurcation diagram in Fig. 1a of Tsumoto et al. (2006). We also give the regions of the bistability in

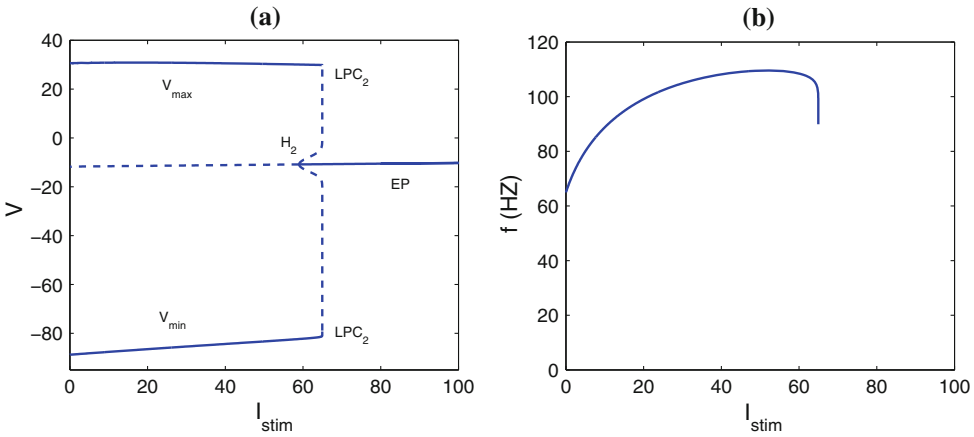

Fig. 8 **a** One-parameter bifurcation diagram along the line l_4 ($\beta_m = -20$). A tangent bifurcation of limit cycle (LPC_2) and a subcritical Hopf bifurcation (H_2) occur. **b** Frequency f as a function of I_{stim}. The frequency at the transition "spiking→ resting" stops at a nonzero value, and it is a Class 2 spiking

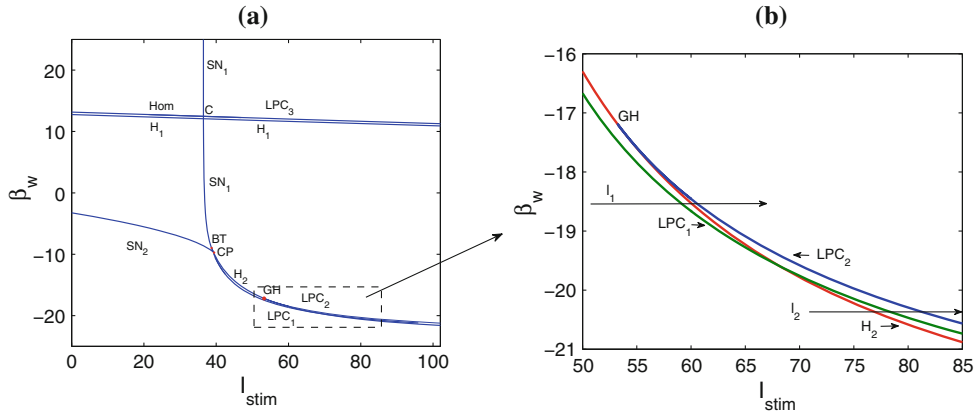

Fig. 9 **a** Two-parameter bifurcation diagram in the (I_{stim}, β_w)-plane. All parameters are as indicated in Sect. 2 with $\beta_m = -1.2$ mV and $\gamma_w = 10$ mV. In addition to the part in the *dashed box*, the other parts of the figure are similar to Fig. 1a of Tsumoto et al. (2006) **(b)** an enlarged bifurcation diagram in the *dashed box* of **a**. The *red, dark green, blue curves* denote Hopf, LPC_1, and LPC_2 *curves*, respectively. $\beta_w = -18.5$ in l_1 and $\beta_w = -20.5$ in l_2 (color figure online)

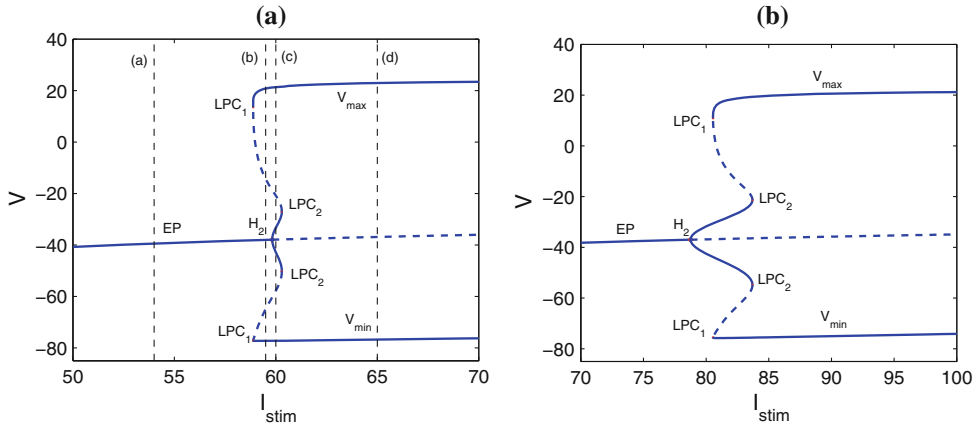

Fig. 10 **a** One-parameter bifurcation diagram along the line l_1 in Fig. 9b ($\beta_w = -18.5$). The *vertical dashed lines* represent $I_{stim} = 54, 59.5, 60, 65$, respectively. There is a bistability in the range between the tangent bifurcation point LPC_1 and LPC_2. When the value of I_{stim} increases between the points LPC_1 and H_2, a stable limit cycle coexists with a stable equilibrium point. When I_{stim} increases from H_2 to LPC_2, two stable limit cycles coexist. **b** One-parameter bifurcation diagram along the line l_2 in Fig. 9b. There is a bistability in the range between the tangent bifurcation points LPC_1 and LPC_2. Two stable limit cycles coexist

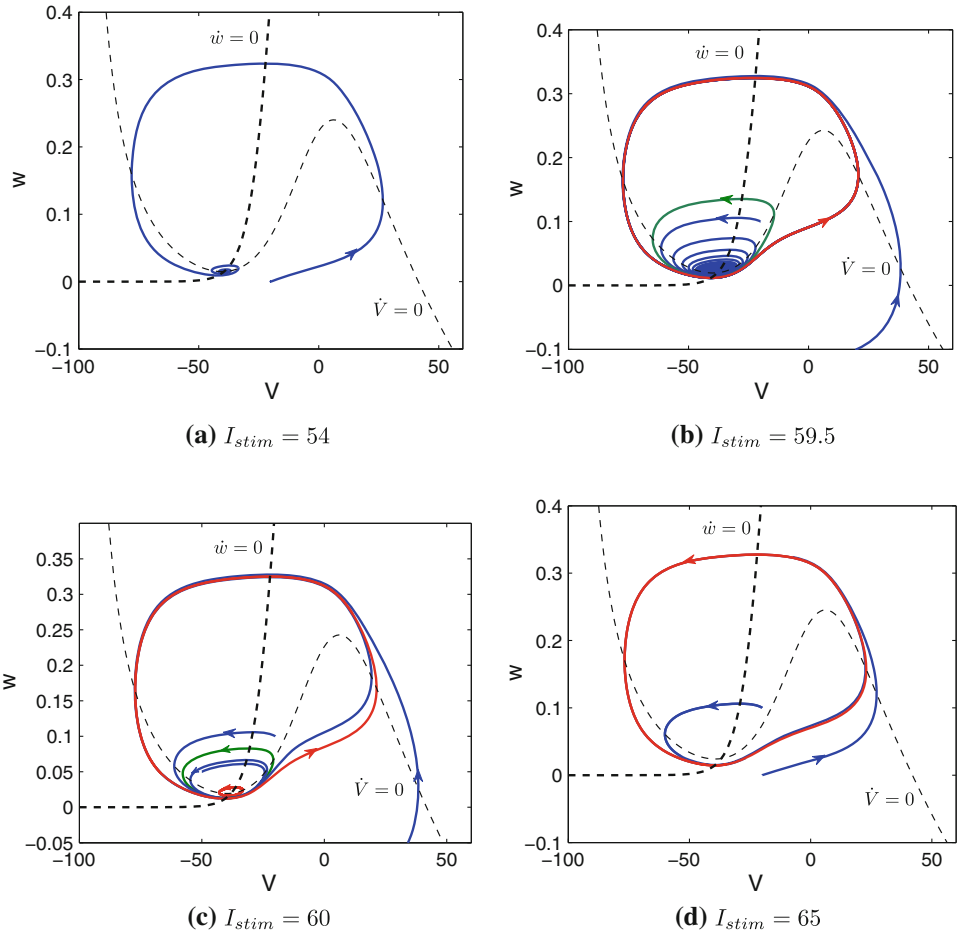

Fig. 11 Examples of phase portraits when $\beta_w = -18.5$. The *red and dark green closed curves* in **b**, **c**, and **d** represent stable and unstable limit cycles, respectively (color figure online)

Fig. 10a, b of model (1). Our results show that there exist three limit cycles of model (1) for some parameters. This is a new dynamical phenomenon in the Morris–Lecar models.

Acknowledgments This work was supported by the National Natural Science Foundation of China (Grant No. 11172103). The authors are grateful to the referees for their valuable suggestions, which helped us to improve the manuscript.

References

FitzHugh R (1955) Mathematical models of threshold phenomena in the nerve membrane. Bull Math Biophys 7:252–278

Guckenheimer J, Holmes P (1983) Dynamical systems and bifurcations of vector Fields. Nonlinear oscillations. Springer, New York

Gutkin BS, Ermentrout GB (1998) Dynamics of membrane excitability determine interspike interval variability: a link between spike generation mechanisms and cortical spike train statistics. Neural Comput 10:1047–1065

Hodgkin AL (1948) The local electric changes associated with repetitive action in a non-medullated axon. J Physiol 107:165–181

Izhikevich EM (2000) Neural excitability, spiking and bursting. Int J Bifurcation Chaos 10:1171–1266

Izhikevich EM (2007) Dynamical systems in neuroscience. MIT Press, Cambridge, MA

Kepler TB, Abbott LF, Marder E (1992) Reduction of conductance-based neuron models. Biol Cybern 66:381–387

Koch C (1999) Biophysics of computation. Oxford University Press, New York

Kuznetsov YA (1998) Elements of applied bifurcation theory, 2nd edn. Springer, New York

Kuznetsov et al (2010) MATCONT is available at http://www.matcont.ugent.be

Morris C, Lecar H (1981) Voltage oscillations in the barnacle giant muscle fiber. Biophys J 35:193–213

Prescott SA, De Koninck Y (2002) Four cell types with distinctive membrane properties and morphologies in lamina I of the spinal dorsal horn of the adult rat. J Physiol 539:817–836

Prescott SA, De Koninck Y, Sejnowski TJ (2008) Biophysical basis for three distinct dynamical mechanisms of action potential initiation. PLOS Comput Biol 4:1–18

Rinzel J, Ermentrout GB (1989) Analysis of neural excitability and oscillations. In: Koch C, Segev I (eds) Methods in neuronal modeling: from Ions to networks. MIT Press, Cambridge, MA, pp 251–291

Sculptoreanu A, De Groat WC (2007) Neurokinins enhance excitability in capsaicin-responsive DRG neurons. Exp Neurol 205: 92–100

Smith PH (1995) Structural and functional differences distinguish principal from nonprincipal cells in the guinea pig MSO slice. J Neurophysiol 73:1653–1667

Tsuji S, Ueta T et al (2007) Bifurcations in two-dimensional Hindmarsh–Rose type model. Int J Bifurcation Chaos 17:985–998

Tsumoto K, Kitajima H et al (2006) Bifurcations in Morris–Lecar neuron model. Neurocomputing 69:293–316